Theory of the coherent decay of high-lying Rydberg states in beam-foil encounters

Tamar Seideman and Moshe Shapiro

Department of Chemical Physics, The Weizmann Institute, Rehovot 76100, Israel

Zeev Vager

Department of Nuclear Physics, The Weizmann Institute, Rehovot 76100, Israel

Theory for the generation and decay of high-lying Rydberg states in beam-foil experiments is presented. Our theory is designed to check the assumption that electron capture in the foil proceeds via a direct transition from a free state. The success of the theory in explaining the observed (primary and secondary) oscillatory structure and underlying smooth background of the ionization signal, as a function of additional variable electric fields, justifies this assumption. In addition, existence of asymmetry with respect to sign change of the variable fields is predicted to be detectable at high field values. Generation of Rydberg atoms in beam-foil experiments is shown to be a sensitive probe of the state distribution prepared during the beam's passage through the foil. Our theory substantiates the claim that Rydberg atoms produced in the beam-foil encounter exit the foil in a pure superposition state.

I. INTRODUCTION

Much work, both experimental and theoretical, has been devoted to the generation of high-lying Rydberg states of hydrogen by electron-capture processes.[1-6] This process is closely related to the problem of the hydrogen atom in an electric field[7-18] because of the extensive use of field ionization in probing Rydberg atoms.

Beam-foil experiments constitute one of the most versatile techniques for studying highly excited Rydberg atoms. In the experiment of Vager et al.,[19] depicted in Fig. 1, a beam of Rydberg atoms is generated by bombardment of a carbon foil with a flux of ions. In order to probe the Rydberg states thus created, the beam is directed through a variable-field region before being ionized in a field spectrometer. The observation of greatest interest is that of a beat pattern in the ionization signal as a function of the variable field strength.[19] The oscillations, which are superimposed on a broad continuum, were attributed to the coherent beating of one Stark sublevel against another.[19] The apparent symmetry of the ionization-yield curve, with respect to the sign of the variable field, and the scarcity of higher harmonics in the oscillatory pattern, were first interpreted[19(a)] to imply that $n_1 \sim n_2$ Stark sublevels are predominantly produced.

This paper is an attempt to elucidate the production mechanism and nature of states generated in the beam-foil encounter. This is done by (a) assuming a specific model and (b) comparing the calculated and observed ionization curves. The success of the latter verifies the inherent assumptions and approach of the former.

In the model presented below we consider three stages of time evolution, (1) preparation of a coherent wave packet in the foil, followed by (2) internal beatings accompanied by slow ionization in the variable electric field, and (3) ionization in the field spectrometer. At each stage we analyze the wave packet in terms of Stark hydrogenic

states, expressed in parabolic as well as spherical coordinates. The main mathematical tool used for calculating energy levels and ionization rates, is the "primitive" WKB theory, whose use is justified due to the high quantum numbers involved. In spite of its simplicity, this model appears to be quantitatively correct, as shown below.

In Sec. II we review some of the theoretical background, in the subjects of electron-transfer processes and the Stark effect. Section III describes our model, and in Sec. IV we present the numerical results and compare them with the experimental findings.

Atomic units are used throughout the work.[20] The unit of time is $\hbar^3/me^4 = 2.4189 \times 10^{-17}$ sec (m being the electron mass); the unit of electric field strength is
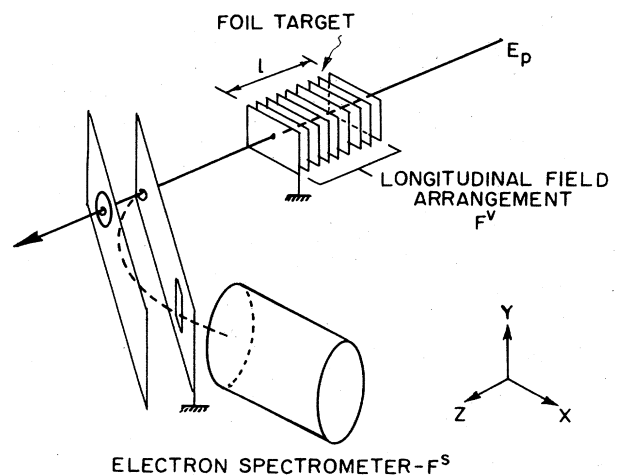
FIG. 1. The experimental set up of Ref. 19. $F^s = 680$ V/cm, $l = 1.7$ cm, $E_p = 3$ MeV, with which time in the variable field $\tau = 0.71$ nsec.

$m^2 e^5/\hbar^4 = 5.142 \times 10^9$ V/cm; and the unit of energy is $me^4/\hbar^2 = 27.21$ eV.

II. THEORETICAL BACKGROUND: CHARGE-EXCHANGE AND BEAM-FOIL EXPERIMENTS

The theory of electron capture into bound states was analyzed within the framework of classical mechanics by Thomas,[21] as early as 1927. His mechanism consists of a two-step process in which the electron is first scattered by the projectile nucleus, then, moving with a speed very close to that of the scatterer, it is scattered again by the target nucleus, with no change of speed. Finally, the mutual attraction between the electron and the projectile serves to bind them.

The first quantum-mechanical treatment is that of Oppenheimer[22] and Brinkman-Kramers[23] (OBK) who only considered electron capture into the ground state of hydrogen. The OBK method was later extended by a number of authors to treat excited states.

The experimental aspect of such charge-transfer processes were reviewed by Tawara and Russek.[24] Shakeshaft and Spruch[3] reviewed the subject of charge transfer with emphasis on the determination of the velocity dependence of the cross section. Their analysis was mainly concerned with exchange of light particles between two colliding heavy nuclei. More recent beam-gas experiments have mostly utilized radiation anisotropy and polarization as a means of revealing asymmetries of the collision process.[25] The alignment (that is, the ratio of magnetic substates cross sections), reflected in such studies, provides in turn fundamental information about the collision.

The ion-atom collision was treated in a number of theoretical studies[1,2,26,27] where the dependence of the charge-exchange cross sections on orbital momentum was analyzed. The majority of numerical calculations of this type were done on the $H^+ + H$ system,[2] some[1] on $H^+ + Ar$, and some on the $H^+ + He$ system.[26,27(b)] All these theories predict a $1/n^3$ dependence of the capture cross section, with predominance of capture into low-angular-momentum states. At the low impact energies (10—100 keV) $n = 0, 1, 2$ states are produced with $n = 1$ the largest. At higher energies the $n = 0$ state dominates.

The beam-foil encounter is more involved and less well understood. Proton—carbon-foil collisions in the 0.5—2.8-MeV range were considered by Lucas et al.,[4] who formulated an empirical theory. Betz et al.[28] investigated the production of Rydberg states in ion-foil collisions, using 125-MeV sulfur and oxygen ions. Their model predicts population of high-angular-momentum states, which was also found experimentally. Supporting evidence to the production of high-l states was provided by the experimental study of Rothermel et al.[5] The two major techniques currently employed for the experimental study of ion excitation and dissociation upon collision with foils are Coulomb explosion spectroscopy[29] and beam-foil spectroscopy.[30] The former[29] has been shown to provide accurate geometric structures of the projectile ions. The latter[30] (i.e., the measurement of the emission spectra of the beam ions as a function of distance behind

the foil) allows one to determine energy levels and lifetimes associated with the observed spectroscopic transitions. Recent theoretical investigations have been mostly concerned with the description of specific systems. The excited-state populations of carbon ions emerging from foil targets was calculated in Ref. 31. Various beam energies were considered, as were a range of carbon-foil thicknesses. Reference 6 proposed a model for the production of the $n = 2$ level of hydrogen, which explained the observed enhancement of Lyman-α radiation following the H_2^+ ions dissociation. The foil structure was, however, not included.

Roughly speaking, the same n^{-3} distribution of final Rydberg states found in the isolated collision case is also found for the beam-foil case. The distribution of Stark sublevels may, however, be quite different.

III SEMICLASSICAL WAVE-PACKET DYNAMICS

A. Preparation stage

The wave packet of Rydberg atoms emerging from the foil, is described as a linear combination of parabolic hydrogenic wave functions, quantized along the proton-beam (z) direction,

$$\Psi(t = 0) = \sum_{\bar{n}_z} C_{\bar{n}_z} \psi_{\bar{n}_z} , \tag{1}$$

where the summation is over the set of quantum numbers $\bar{n}_z = \{n, n_{2z}, m_z\}$ characterized by the quantization direction.

Because the electron capture is a very fast process, the expansion coefficients are factorizable as overlap integrals between plane-wave functions for the free-electron and hydrogenic wave functions of the bound electron times a constant average potential. Thus up to a constant (see also Refs. 24 and 25),

$$C_{\bar{n}_z} = \langle \psi_{\bar{n}_z} \mid \exp(ikz) \rangle$$
$$= \int_0^{2\pi} \int_0^\infty \int_0^\infty \psi_{n,n_2,0}(\xi, \eta, \phi)(2\pi)^{-1/2}$$
$$\times \exp[ik(\xi - \eta)/2]$$
$$\times \tfrac{1}{4}(\xi + \eta) d\xi \, d\eta \, d\phi , \tag{2}$$

where the parabolic coordinates ξ, η, ϕ are defined by[32]

$$\xi = R + Z, \quad \eta = R - Z, \quad \phi = \tan^{-1}(Y/X) \tag{3}$$

with

$$0 \le \xi, \eta, \quad 0 \le \phi \le 2\pi .$$

ψ are solutions of the hydrogen in a uniform electric field problem,

$$(\tfrac{1}{2}\Delta + E + 1/R - FZ)\psi = 0 . \tag{4}$$

In parabolic coordinates ψ separates to the product form

$$\psi = \chi_1(\xi)\chi_2(\eta)\exp(im\phi) ,$$
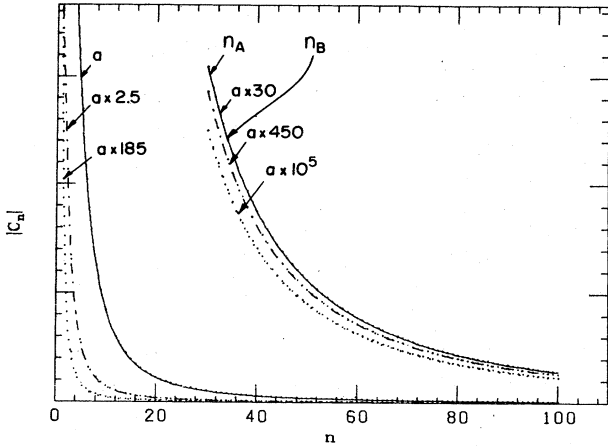
FIG. 2. Principal-quantum-number distribution. $n_A \leq n \leq n_B$ denotes the range of tunneling energy levels. [$|C_n|$ is the absolute value of the preparation coefficient as given by Eq. (8).] Relative energy: ———, $E = 0.25$ a.u.; —·—·—·, $E = 1.0$ a.u.; ···, $E = 16.0$ a.u.

where

$$\chi_1 = (\epsilon\xi)^{1/2} f_{n_1,m}(\epsilon\xi)$$

$$\chi_2 = (\epsilon\eta)^{1/2} f_{n_2,m}(\epsilon\eta) ,$$

(5)

where $\epsilon = (-2E)^{1/2}$ and $f_{p,m}$ are solutions of the one-dimensional equations

$$(d/d\xi)(\xi\, df_1/d\xi) + (E\xi/2 + \beta_1)f_1 = 0 ,$$

(6a)

$$(d/d\eta)(\eta\, df_2/d\eta) + (E\eta/2 + \beta_2)f_2 = 0$$

(6b)

with $\beta_1 + \beta_2 = 1$.

In the above $m = 0$ because of the present choice of quantization axis. The integral may be explicitly evaluated[33] to yield

$$C_{\bar{n}_z} = |C_n| \exp(i\alpha_{\bar{n}}) ,$$

(7)

where

$$|C_n| = 32^{1/2} n^2 / (1 + k^2 n^2)^2 ,$$

$$\alpha_{\bar{n}} = (n_2 - n_1) \tan^{-1}[2kn/(k^2 n^2 - 1)] .$$

(8)

For $(kn)^2 \gg 1$, we find that the amplitude behaves as $32^{1/2}/k^4 n^2$. The n dependence of the total capture cross section,

$$\sigma^{(n)} \sim \sum_{n_2} |C_n|^2 \sim 1/n^3 ,$$

(9)

is thus in agreement with the generally accepted n^{-3} scaling law.

This simple state distribution is described in Fig. 2. Only the states indicated as $n_B \geq n \geq n_A$ are probed by the field spectrometer. Lower states cannot be ionized within the 10^{-10} sec of residence time in the spectrometer, while for higher states all sublevels lie above the potential barrier in the variable field, again not contributing to the yield.

It is also of interest to express the initial wave packet in terms of the more commonly used spherical representation. The results, shown in Fig. 3, are obtained by expanding the parabolic hydrogenic functions in the spherical ones,

$$\psi_{n,n_2,m}(\xi,\eta,\phi) = \sum_l \langle \psi_{n,l,m} | \psi_{n,n_2,m} \rangle \psi_{n,l,m}(R,\theta,\phi) , \quad (10)$$

and substituting in Eq. (1). The expansion coefficients of Eq. (10) are given analytically as

$$\langle \psi_{n,l,m} | \psi_{n,n_2,m} \rangle = (-1)^{K - k_1 + l + m} (K\,K\,l\,m \,|\, K\,k_1\,K\,k_2) ,$$

(11)

where $(K\,K\,l\,m \,|\, K\,k_1\,K\,k_2)$ are Clebsch-Gordan coefficients[34] and

$$k_1 = (m + n_1 - n_2)/2, \quad k_2 = (m - n_1 + n_2)/2 . \quad (12)$$

The above formula is essentially that derived by Park[35] save for the $(-1)^{K - k_1 + l + m}$ phase factor, omitted by him.

The separation of variables in parabolic coordinates is formally equivalent to the introduction of two angular momenta $\mathbf{J}_1^{(n)}$ and $\mathbf{J}_2^{(n)}$, where
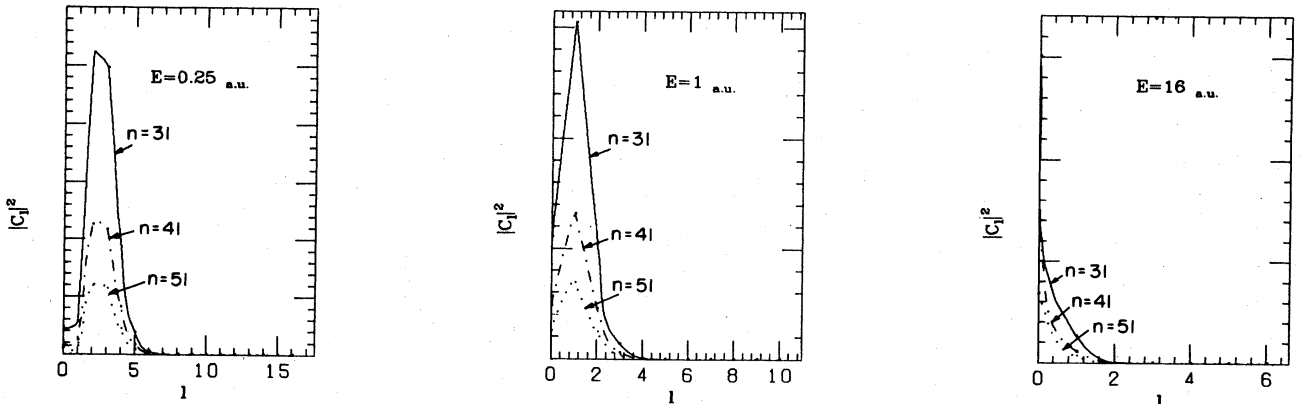
FIG. 3. Angular-momentum-state distribution.

$$\mathbf{J}_1^{(n)}=\tfrac{1}{2}\mathbf{L}-q_n\mathbf{A}, \quad \mathbf{J}_2^{(n)}=\tfrac{1}{2}\mathbf{L}+q_n\mathbf{A} \tag{13}$$

with $\mathbf{L}$ the orbital angular momentum, and $\mathbf{A}$ the Lentz vector,

$$\mathbf{A}=\tfrac{1}{2}(\mathbf{p}\times\mathbf{L})-\tfrac{1}{2}(\mathbf{L}\times\mathbf{p})-r^{-1}\mathbf{r} . \tag{14}$$

Thus the transformation from parabolic to spherical coordinates amounts to a change in representation equivalent to the addition of $\mathbf{J}_1^{(n)}$ and $\mathbf{J}_2^{(n)}$ to form $\mathbf{L}$.

As shown in Fig. 3, the higher the wave number, the more isotropic is the distribution. A direct evaluation of the overlap integral between a plane wave and the spherical coordinates wave function shows that the cross section scales as $1/k^{2l+2}$ (see Ref. 33 for more details).

B. Energy eigenvalues and ionization rates in a weak electric field

After preparation the wave packet is subjected (see Fig. 1) to two external electric fields, a weak variable field and the strong spectrometer field. The time evolution of the wave packet is given as

$$\Psi(t)=\sum_{\bar{n}}[C_{\bar{n}}\psi_{\bar{n}}\exp(-iE_{\bar{n}}^Vt-W_{\bar{n}}^Vt/2)], \tag{15}$$

where the $C_{\bar{n}}$ are the preparation coefficients, discussed in Sec. III A. In what follows we will denote by V and S all values related to the variable and spectrometer field, respectively. Thus $E_{\bar{n}}^V$ and $W_{\bar{n}}^V$ are the eigenvalue and ionization rate of each Stark sublevel in the field V.

In order to follow the dynamics we need an efficient way of calculating $E_{\bar{n}}^V$ and $W_{\bar{n}}^V$. To this end we applied the primitive WKB approximation. Although there are more accurate methods for special sets of quantum numbers, such as the uniform semiclassical techniques,[15,16] we chose to follow the primitive semiclassical method because the simple formulas derived below are uniformly applicable over a wide range of quantum numbers.

We start the development by noting that the electric field mainly affects $\mathcal{X}_2(\eta)$ and has very little effect on $\mathcal{X}_1(\xi)$. We can approximate $\mathcal{X}_1(\xi)$ as a pure hydrogenic wave function $\mathcal{X}_1(\xi)=(\epsilon\xi)^{1/2}f_{n_1,m}^H(\epsilon\xi)$, where

$$f_{p,m}^H(R)=1/|m|![(p+|m|)!/p!]^{1/2}F(-p,|m|+1,R)\exp(-R/2)(R)^{|m|/2} . \tag{16}$$

The ionization probability of a single Stark sublevel is mainly determined by $\mathcal{X}_2(\eta)$ at large values of η (corresponding to large negative z). Solving Eq. (6b) in the WKB approximation, one has

$$\mathcal{X}_2(\eta)=f_{n_2,m}^H(\epsilon\eta_0)(\eta_0|p_0|/p)^{1/2}$$
$$\times \exp\left[i\int p(\eta')d\eta'-3\pi i/4\right], \tag{17}$$

where $p(\eta)$ is the "local" semiclassical momentum, given in the Langer modification[36] as

$$p(\eta)=[2(E-U)]^{1/2}$$
$$=(E/2+\beta_2/\eta-m^2/4\eta^2+F\eta/4)^{1/2} . \tag{18}$$

The $f_{n_2,m}^H(\epsilon\eta_0)$ factor guarantees that the WKB wave function is properly normalized. This is done by equating it to the true wave function at one point $\eta=\eta_0$, where $1/\epsilon\ll\eta_0\ll\epsilon^2/F$, F being the field intensity. The point η_0 is chosen to be inside the barrier but sufficiently close to the nucleus such that the external potential is still negligible. At that point the true wave function can be safely replaced by $f_{n_2,m}^H$. The integral $\int p(\eta)d\eta$ may include a (tunneling) region $\eta_0<\eta<\eta_1$, η_1 being the outer root of the equation $p(\eta)=0$, where $p(\eta)$ is imaginary. This gives rise to the familiar tunneling damping factor in the action integral [Eq. (17)].

Evaluation of the action integral and use of the asymptotic form of the Laguerre polynomials[37] leads to the following expression for the probability density at large values of η:

$$|\psi|^2=(n^4\pi)^{-1}[f_{n_1,m}(\xi/n)]^2$$
$$\times[(n_2+|m|)!n_2!p(\eta)]^{-1}(4\epsilon^3/F)^{(2\beta/\epsilon)}$$
$$\times \exp(-2\epsilon^3/3F)/\eta . \tag{19}$$

The ionization current is given by the flux through a plane perpendicular to the z axis. In the WKB approximation it assumes the simple form

$$W=\int_0^{2\pi}d\phi\int_0^\infty r\,dr\,\psi v_z\psi^*=\int_0^\infty \psi v_z\psi^*2\pi r\,dr , \tag{20}$$

where r is the distance of a given point on the plane from the z axis, $r=(X^2+Y^2)^{1/2}=(\xi\eta)^{1/2}$, and v_z is the component of the velocity in the z direction. Writing

$$dr=\tfrac{1}{2}(\eta/\xi)^{1/2}d\xi \quad (\eta\gg\xi)$$

we obtain

$$W=\int_0^\infty \mathcal{X}v_z\mathcal{X}^*\pi d\xi$$
$$=[n^3(n_2+|m|)!n_2!]^{-1}(4\epsilon^3/F)^{(2\beta/\epsilon)}$$
$$\times \exp(-2\epsilon^3/3F) , \tag{21}$$

where we used the normalization of $f_{p,m}^H$. The implicit dependence of β, the separation constant, on the energy is determined by the Bohr-Sommerfeld quantization rule,

$$\int p(E,\beta_1,\xi)d\xi=(n_1+\tfrac{1}{2})\pi , \tag{22a}$$

$$\int p(E,1-\beta_1,\eta)d\eta=(n_2+\tfrac{1}{2})\pi , \tag{22b}$$

where $p(E,\beta,\eta)$ is defined in Eq. (18). The action integrals can be reduced to complete elliptic integrals.[9,13] We chose, however, to determine E and β iteratively, by expanding both equations (22) as derivative series. As initial values for the iteration we use the fourth-order perturbation expressions of Alliluev and Malkin[8] for E and β. The action integrals and their β derivatives were evaluated using a Gauss-Mehler quadrature scheme, a method which proved extremely efficient in the evaluation of similar integrals in the past.[38]

Extensive comparisons show that the primitive semi-

classical formulas outlined here are very reliable: At low and intermediate field strengths, the eigenvalues and ionization rates thus generated agree, to within a few percent, with more exact methods.[7,8,14-16] We have used this method in the calculations reported below.

C. Propagation in time through the Z-parallel electric fields

In the first configuration considered, both fields are directed parallel to the proton beam. The weak variable field is applied immediately after the exit from the foil.

On entering the variable-field (F^V) region, the wave packet is given by Eq. (1). At subsequent time t, it assumes the form

$$\Psi(t) = \sum_{\bar{n}} C_{\bar{n}} \psi_{\bar{n}} \exp(-iE_{\bar{n}}^V t - W_{\bar{n}}^V t/2) , \tag{23}$$

where $W_{\bar{n}}^V$ is given by Eq. (21) and $E_{\bar{n}}^V$ is determined by the quantization conditions Eq. (22).

The wave packet exits from the variable field at time $t = \tau$, and propagates for an additional time t_1 subject to the influence of the spectrometer field (F^S),

$$\Psi(\tau + t_1) = \sum_{\bar{n}} |C_n| \psi_{\bar{n}} \exp[-i(E_{\bar{n}}^V \tau + E_{\bar{n}}^S t_1 - \alpha_{\bar{n}})$$
$$- (W_{\bar{n}}^V \tau + W_{\bar{n}}^S t_1)/2] , \tag{24}$$

where we substituted $C_{\bar{n}} = |C_n| \exp(i\alpha_{\bar{n}})$.

As in Eq. (20) the ionization current for the nonstationary wave packet is given as an integral over flux

$$W^{(z)}(t) = \int_0^\infty \Psi(t) v_z \Psi^*(t) 2\pi r \, dr$$

$$= \sum_{\bar{n}\bar{n}'} |C_n||C_{n'}| \left[\int_0^\infty \psi_{\bar{n}} v_z \psi_{\bar{n}}^* 2\pi r \, dr \right]$$

$$\times \exp[-i(E_{\bar{n}}^V \tau + E_{\bar{n}}^S t_1 - \alpha_{\bar{n}'} - E_{\bar{n}}^V \tau - E_{\bar{n}}^S t_1 + \alpha_{\bar{n}'}) - (W_{\bar{n}}^V \tau + W_{\bar{n}}^S t_1 + W_{\bar{n}'}^V \tau + W_{\bar{n}'}^S t_1)/2] . \tag{25}$$

Analogous to the evaluation of the diagonal elements we set

$$I_{\bar{n}\bar{n}'} = \int_0^\infty \psi_{\bar{n}} v_z \psi_{\bar{n}}^* 2\pi r \, dr$$

$$= (n^2 n'^2 n_2! n_2'!)^{-1} (4\epsilon^3/F)^{(\beta/\epsilon)} (4\epsilon'^3/F)^{(\beta'/\epsilon')} \exp[-(\epsilon^3 + \epsilon'^3)/3F]$$

$$\times \int_0^\infty F(-n_1, 1, \xi/n) F(-n_1', 1, \xi/n') \exp[-(\xi/n + \xi/n')/2] d\xi . \tag{26}$$

The integral over ξ, denoted $J_{\bar{n}\bar{n}'}$, can be shown[33] to yield

$$J_{\bar{n}\bar{n}'} = (-1)^{n_1} [2nn'/(n'+n)][(n'-n)/(n'+n)]^{(n_1'-n_1)} P_{n_1}^{0,(n_1'-n_1)} (1 - 8nn'/(n+n')^2) \quad (n_1' > n_1) , \tag{27}$$

where $P_n^{(\alpha,\beta)}(x)$ is the Jacobi polynomial. It should be noted that for $n = n'$ this integral reduces to a δ function,

$$J_{n_1,n_1'} = \int_0^\infty F(-n_1, 1, \xi/n) F(-n_1', 1, \xi/n) \exp(-\xi/n) d\xi = n\delta_{n_1,n_1'} . \tag{28}$$

This results from the orthogonality of the basis functions with respect to n_1 (for more details see Ref. 33).

Use of Eqs. (26) and (27) in Eq. (25), and integration over time in the spectrometer field, gives

$$W^{(z)} = \int_0^T W^{(z)}(t) dt \tag{29}$$

$$= \sum_{\bar{n}\bar{n}'} |C_n||C_{n'}| (W_{\bar{n}}^S W_{\bar{n}'}^S/nn')^{1/2} J_{\bar{n}\bar{n}'}$$

$$\times [\exp(-i\Delta E^s - \Gamma^s)T - 1](i\Delta E^s - \Gamma^s) \exp(-i\Phi - \Gamma_\tau^v)/[(\Delta E^s)^2 + (\Gamma^s)^2] ,$$

where

$$W_{\bar{n}}^S = [n^3 (n_2!)^2]^{-1} \exp(-2\epsilon^3/3F^s)(4\epsilon^3/F^s)^{(2\beta/\epsilon)} ,$$

$$\Gamma^s = (W_{\bar{n}}^S + W_{\bar{n}'}^S)/2, \quad \Gamma^v = (W_{\bar{n}}^V + W_{\bar{n}'}^V)/2 , \tag{30}$$

$$\Delta E^s = E_{\bar{n}}^S - E_{\bar{n}'}^S, \quad \Phi = E_{\bar{n}}^V \tau - E_{\bar{n}'}^V, \quad \tau - \alpha_{\bar{n}} + \alpha_{\bar{n}'} .$$

Or, in real form,

$$W^{(z)} = \sum_{\bar{n} \neq \bar{n}'} A_{\bar{n}\bar{n}'} \{ [\exp(-\Gamma^s T) \cos(\Delta E^s T) - 1](\Delta E^s \sin\Phi - \Gamma^s \cos\Phi)$$

$$+ \exp(-\Gamma^s T) \sin(\Delta E^s T)(\Delta E^s \cos\Phi + \Gamma^s \sin\Phi) \} + W_d^{(z)} , \tag{31}$$

where $W_d^{(z)}$ is the contribution of terms of equal principal quantum numbers $(n = n')$,

$$W_d^{(z)} = \sum_n \sum_{n_2} |C_n|^2 \exp(-W_{\bar{n}}^V \tau)[1 - \exp(-W_{\bar{n}}^S T)]$$

(32)

and

$$A_{\bar{n}\bar{n}'} = |C_n||C_{n'}|(W_{\bar{n}}^S W_{\bar{n}'}^S / nn')^{1/2} J_{\bar{n}\bar{n}'}$$

$$\times \exp(-\Gamma^v \tau)/[(\Delta E^s)^2 + (\Gamma^s)^2] .$$

(33)

$A_{\bar{n}\bar{n}'}$ has the familiar Lorentzian shape, multiplied by the decaying exponent $\exp(-\Gamma^v \tau)$, which indicates the loss of yield in the spectrometer due to ionization in the variable field. As noted above [Eq. (28)], when both fields are parallel to the z axis, the only interference effect must come from terms with different principal quantum numbers. These interferences are weak, hence we expect a rather smooth nonoscillatory dependence of the ionization rate on the variable-field strength.

In order to compare our theory with experiments we must also consider the background (nonoscillatory) current. It is due to Rydberg states whose energy is below the ionization barrier in the weak variable field, but above that barrier in the strong spectrometer field. Clearly we must reexamine the meaning of the so-called "states" entering the spectrometer field.

Strictly speaking, the Stark Hamiltonian has no discrete eigenvalues. Even in the presence of an infinitesimal uniform field the spectrum becomes continuous, and the discrete levels are really narrow resonances. If the energies of these resonances are well below the ionization barrier, the treatment above and the resonance picture are identical. If the resonances broaden, as they must above the ionization barrier, each such state is actually a wave packet whose initial energy envelope is given by some predetermined preparation process, such as the beam-foil encounter and the passage through the weak longitudinal field. The time evolution of such a wave packet is most readily obtained by expanding it in a basis composed of stationary scattering eigenstates. We then have that

$$\psi_{E_n}(t) = \sum_{\bar{n}} \int dE \, \psi_{\bar{n}}(E)\langle \psi_{\bar{n}}(E) | \psi(t=0)\rangle \exp(-iEt) .$$

(34)

This state is initially (where the initial time is $t = \tau$ and τ is the entrance time to the spectrometer region) a pure hydrogenic wave function which has decayed a bit in the longitudinal variable field. If the resonance is not too wide (i.e., resonances do not yet overlap), we can treat each resonance in isolation. (If resonances do overlap, their combined large energetic width would imply a very fast ionization rate, and all atoms would be ionized during the beam passage in the spectrometer. The signal will then be determined entirely by the fraction of atoms that survived the weak longitudinal field.) For isolated resonances we can parametrize the energy profile of the wave packet as a simple Lorentzian,[39]

$$|A_{\bar{n}}(E)|^2 = |\langle \psi_{\bar{n}}(E) | \psi(t=0)\rangle|^2$$

$$= \Gamma/\{2\pi[(E - E_n)^2 + \Gamma^2/4]\} ,$$

(35)

where E_n is the energy, and Γ the width, of the resonance. We have that

$$\psi_{E_n}(t) = \psi(t=0) \exp(-iE_n t - \Gamma_n t/2) .$$

(36)

We have thus expressed the decay of states above and below the ionization barrier in an identical form. The major difference lies in the values assigned to E_n and Γ. For levels above the ionization barrier these parameters are simply determined by expanding as in Eq. (35) where the initial state is hydrogenic eigenstate and the scattering basis set is made up of the primitive WKB wave functions, at energies above the ionization barrier.

The overall background contribution to the flux can be written as

$$W^{\text{background}} = \sum_{\bar{n} > \bar{n}_c} |C_n|^2 \exp(-W_{\bar{n}}^V \tau)$$

$$\times [1 - \exp(-W_n^c T)] ,$$

(37)

where W_n^c is given by Eq. (A3) of Ref. 33, with $\bar{n}_c = (n, n_2, m)_c$ denoting the sublevel above which all states lie above the ionization barrier in the spectrometer field. As can be seen from Eq. (37) the background term is nonoscillatory and symmetric with respect to a change of sign of the variable field.

The total ionization yield curve for the z-directed parallel fields is shown in Fig. 4. As expected, it is a smooth function of the variable fields: The only interferences are due to states with different principal quantum numbers. As shown below, this will no longer be the case if the fields are tilted with respect to one another. Under these circumstances the strong interference between nearby Stark sublevels is possible.

D. Tilted electric fields

We now wish to consider the experiment under which both or one of the fields is tilted relative to the proton-beam direction. The effect of such a tilt is analyzed by
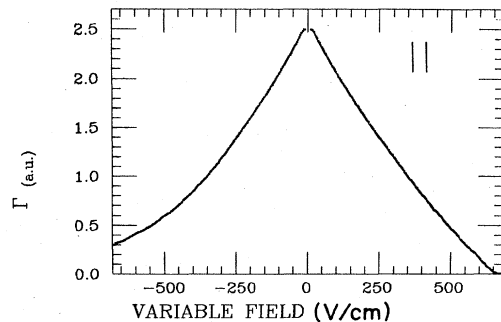
FIG. 4. Ionization-yield curve for fields parallel to the proton-beam direction. The parameters are the same as in Fig. 1.

rotating the quantization axis from the z direction to a new direction (r). We have that

$$\sum_{\bar{n}_z} C_{\bar{n}_z}\psi_{\bar{n}_z} = \sum_{\bar{n}_r} C_{\bar{n}_r}\psi_{\bar{n}_r} \tag{38}$$

and using the orthogonality, we obtain

$$C_{\bar{n}_r} = \sum_{\bar{n}_z} C_{\bar{n}_z}\langle \psi_{\bar{n}_r} | \psi_{\bar{n}_z}\rangle \, , \tag{39}$$

where subscript r is used to denote the rotated frame.

It can be shown[33] that the transformation coefficients of Eq. (39) are given as simple products of rotation matrices,

$$C_{\bar{n}_r} = | C_n | \sum_{k_{1z}} (-1)^{k_{2r}+k_{1r}} d^{(K)}_{k_{1r},k_{1z}}(\theta)$$

$$\times d^{(K)}_{k_{2r},-k_{1z}}(\theta) \exp(-2ik_{1z}\beta_n) \tag{40}$$

with C_n and $\alpha_{\bar{n}}=(n_2-n_1)\beta_n$ given by (8), and θ being the tilt angle.

Referring to the experimental setup in which the variable and the spectrometer fields are both tilted at 45° relative to the initial beam direction, we rewrite the coefficient of each state on entering the second field as

$$C^{(//)}_{\bar{n}_r} = \exp[-i(E^V_{\bar{n}_r}\tau + E^0_n\tau^0) - W^V_{\bar{n}_r}\tau/2]$$

$$\times \sum_{n_{2z}} \langle \psi_{\bar{n}_r} | \psi_{\bar{n}_z}\rangle\langle \psi_{\bar{n}_z} | \exp(ikz)\rangle \, , \tag{41}$$

where τ^0 denotes the short period of time allowed to elapse between the two fields, and E^0_n is the zero-field energy, $E^0_n = -(2n^2)^{-1}$.

For the second setup, where the variable field is along the z axis and the spectrometer field is tilted with respect to it, we have

$$C^{(|/)}_{\bar{n}_r} = \sum_{n_{2z}} \exp[-i(E^V_{\bar{n}_z}\tau + E^0_n\tau^0) - W^V_{\bar{n}_z}\tau/2]$$

$$\times \langle \psi_{\bar{n}_r} | \psi_{\bar{n}_z}\rangle\langle \psi_{\bar{n}_z} | \exp(ikz)\rangle \, , \tag{42}$$
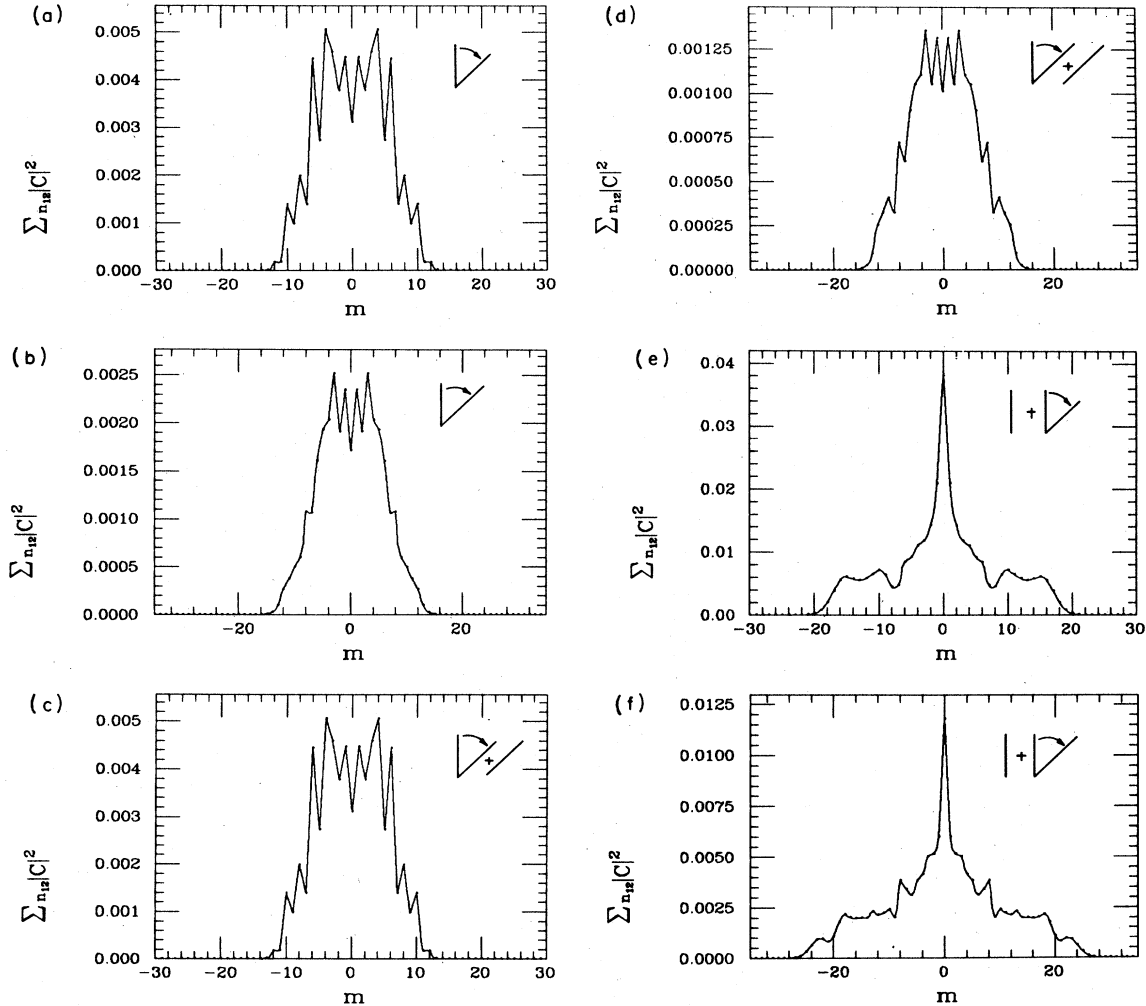
FIG. 5. Magnetic-quantum-number distribution: (a), (c), and (e), $n=31$; (b), (d), and (f), $n=36$; $F=400$ V/cm. (a) and (b) after a 45° rotation; (c) and (d) after a 45° rotation followed by passage through the field region; (e) and (f), after propagation through field parallel to the proton-beam direction, followed by rotation of 45°.

which differs from Eq. (41) in that the time propagation in the first and second fields apply to different sets of quantum numbers.

It is of interest to compare the distribution of m states in the three cases considered: After (a) 45° rotation; (b) 45° rotation followed by propagation through a variable field, also tilted at 45° to the z axis; and (c) propagation through a variable field parallel to the z axis, followed by a 45° rotation. In Figs. 5(a)—5(f) we plot the absolute squared value of the coefficients for each m state (summed over all $n_{12} = n_1 - n_2$), as a function of m. We consider two different principal quantum numbers: $n = 31$ which is only slightly ionized in a 400-V/cm field, and $n = 36$ which is ionized to a considerable extent.

A comparison of Figs. 5(a) and 5(b) with Figs. 5(c) and 5(d) shows that the z component of the angular momentum remains a constant of the motion in the presence of the field: the distribution of m states, prepared in the rotation has not been changed. [Figures 5(b) and 5(d) show the effect of ionization in reducing appreciably all coeffi-

cients. The relatively small change in the distribution is due to the m dependence of the ionization probability.]

The situation is different when the wave functions enter the variable field with $m = 0$ [Figs. 5(e) and 5(f)]. The field effect is to change the initial narrow distribution of l states into a linear combination of all $n - 1$ angular momentum states (i.e., l is not a good quantum number in the presence of the field). The axis rotation now reveals a new distribution of magnetic quantum numbers. In Figs. 6(a)—6(f) we make the analogous comparison for the distribution of n_{12}—the A_z eigenvalues. This, again, demonstrates the qualitative difference between the two experimental configurations. Figure 6(d) clearly shows the field effect in depleting primarily the high-n_2 states (states with high charge distribution in the negative z direction) while the state population in the low-n_2 region remains unaffected.

Contrary to the z-parallel field situation (Sec. III), the tilted-field case is complicated by the presence of more than one m state. At time $t = \tau + \tau^0 + t_1$,
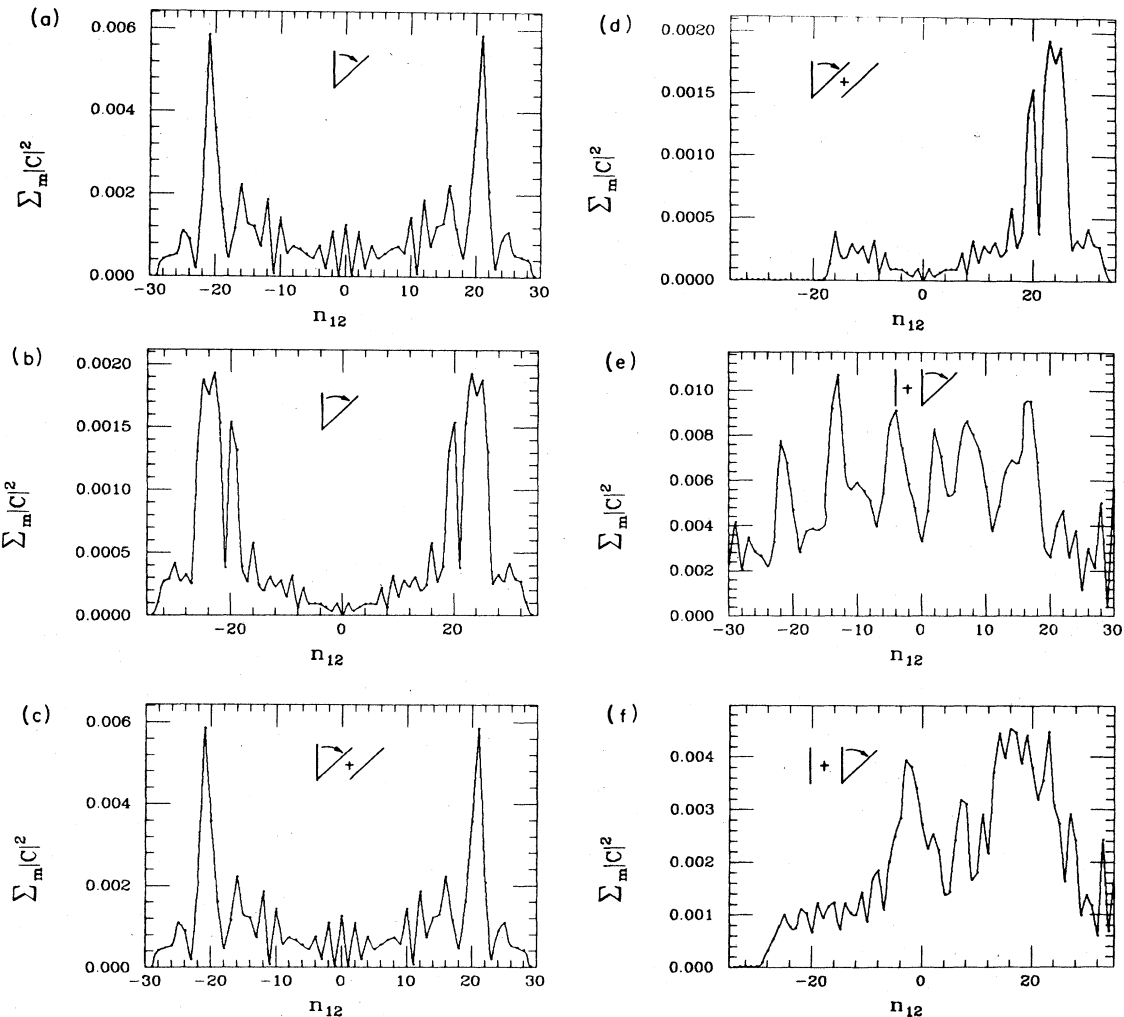
FIG. 6. As in Fig. 5, for $(n_1 - n_2)$, the electric-quantum-number distribution.
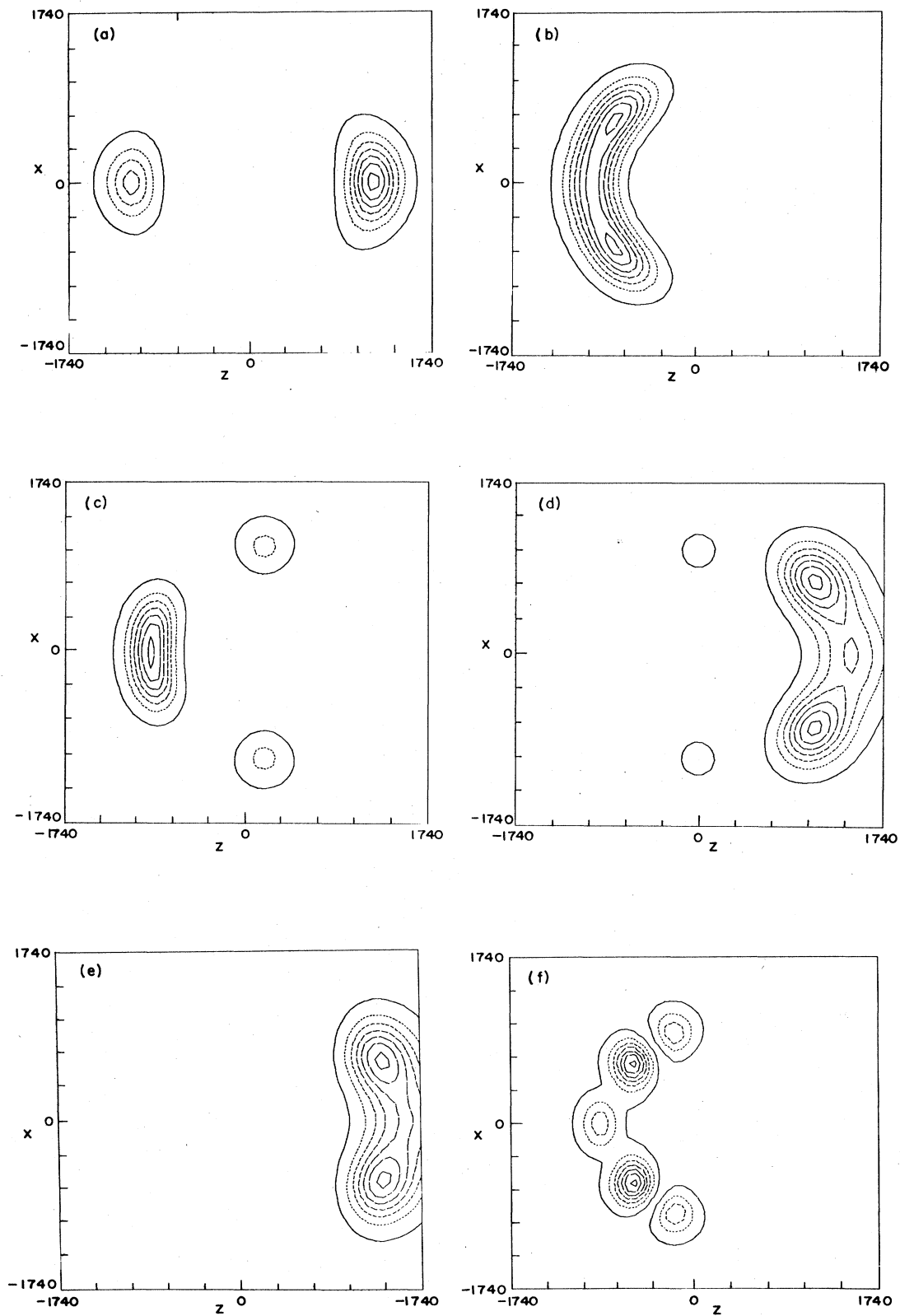
FIG. 7. Probability density upon exit from the variable field at $\tau=0.71$ nsec. (a) $F=50$ V/cm; (b) $F=200$ V/cm; (c) $F=400$ V/cm; (d) $F=500$ V/cm, (e) and (f) ionization in a 680 V/cm spectrometer field, following the passage through (e), a parallel, and (f), an antiparallel 500 V/cm field.

$$\Psi(\tau+\tau^0+t_1)=\sum_{\bar{n}_r} C_{\bar{n}_r}\psi_{\bar{n}_r}\exp[(-iE^S_{\bar{n}_r}-W^S_{\bar{n}_r}/2)t_1] ,$$

$$(43)$$

where $C_{\bar{n}_r}$ is given by Eq. (41) or by Eq. (42). After integrating $W(t)$ over the time, and making use of the orthogonality of the different n_1 and equal energy basis functions, we obtain for the diagonal $(\bar{n}'_r=\bar{n}_r)$ W_d term,

$$W_d=\sum_{\bar{n}_r} C_{\bar{n}_r}C^*_{\bar{n}_r}[1-\exp(-W^S_{\bar{n}_r}T)] .$$

$$(44)$$

By substituting Eq. (41) for $C_{\bar{n}_r}$, we obtain for the parallel-tilted-fields case,

$$W_d^{(//)}=\sum_{\bar{n}_r}\exp(-W^V_{\bar{n}_r}\tau)[1-\exp(-W^S_{\bar{n}_r}T)]$$

$$\times\left|C_n\sum_{n_{2z}}\exp(i\alpha_{\bar{n}_z})\langle\psi_{\bar{n}_r}|\psi_{\bar{n}_z}\rangle\right|^2 .$$

$$(45)$$

When one field is tilted with respect to the other, we substitute Eq. (42) for $C_{\bar{n}_r}$, to obtain

$$W_d^{(|/)}=\sum_{\bar{n}_r}[1-\exp(-W^S_{\bar{n}_r}T)]$$

$$\times\left|C_n\sum_{n_{2z}}\exp[-i(E^Z_{\bar{n}_z}\tau+\alpha_{\bar{n}_z})-W^V_{\bar{n}_z}\tau/2]\right.$$

$$\left.\times\langle\psi_{\bar{n}_r}|\psi_{\bar{n}_z}\rangle\right|^2 .$$

$$(46)$$

Contrary to the parallel-fields case, when the fields are tilted even the W_d term gives rise to a beat pattern associated with changing the variable-field strength. To see this explicitly, we write $W_d^{(|/)}$ using real arithmetic as

$$W_d^{(|/)}=2\sum_{\bar{n}_r}[1-\exp(-W^S_{\bar{n}_r}T)]$$

$$\times|C_n|^2\sum_{n_{2z}\geq n_{2z'}}\langle\psi_{\bar{n}_r}|\psi_{\bar{n}_z}\rangle\langle\psi_{\bar{n}_z'}|\psi_{\bar{n}_r}\rangle$$

$$\times\exp(-\Gamma^v\tau)\cos\Phi ,$$

$$(47)$$

where

$$\Phi=(E^V_{\bar{n}_z}-E^V_{\bar{n}_z'})\tau-\alpha_{\bar{n}_z}+\alpha_{\bar{n}_z'} .$$

$\cos\Phi$ is responsible for the oscillations in the ionization-yield curve.
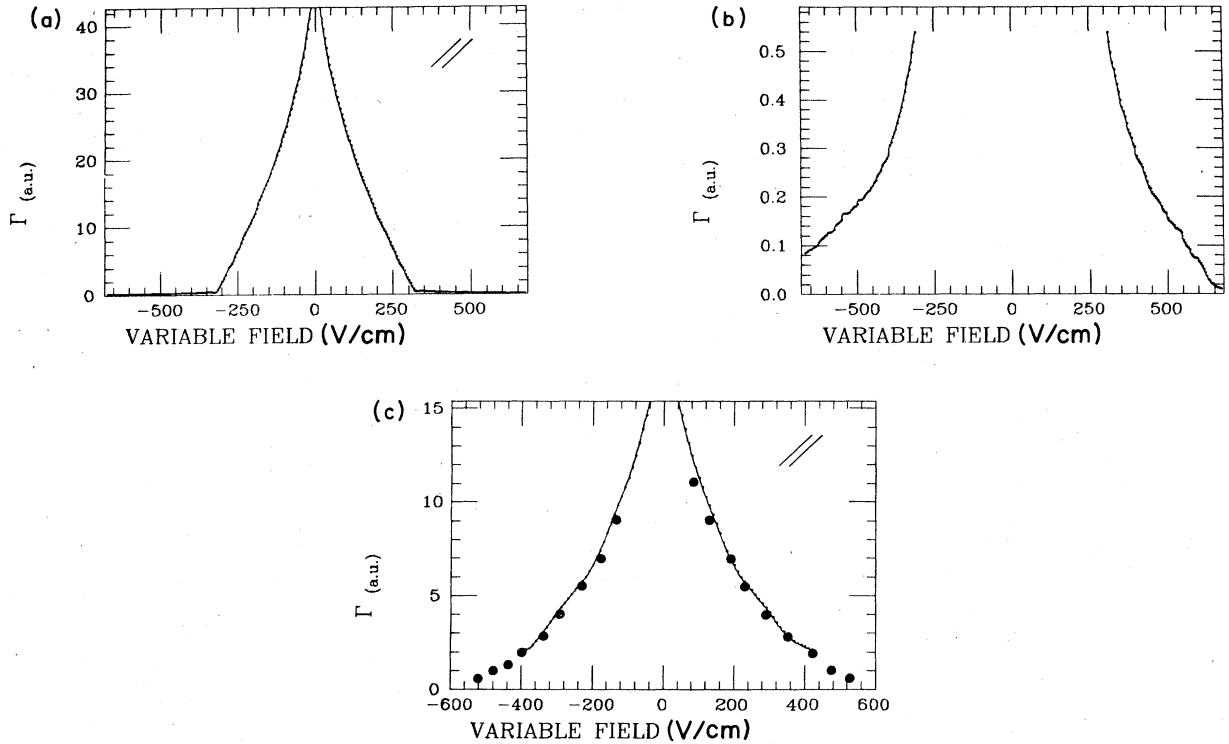
FIG. 8. (a) Ionization yield for mutually parallel fields, tilted with respect to the proton-beam direction. The parameters of Fig. 1 were used. (b) Enlargement of the high-field region, revealing asymmetry. (c) As in (a), with F^s=450 V/cm, E_p=2 MeV, 1=4 cm (for which τ=2.04 nsec) ———, theory; $\cdots$, experiment [Ref. 19(b)].

As in the parallel-fields case, the smooth background is due to levels above the ionization barrier in the spectrometer. The contribution of these levels is given, as in Eq. (34) above, by

$$W^{\text{background}} = \sum_n [1 - \exp(-W_n^c T)] \sum_{n_{2r}, m_r} |C_{\bar{n}_r}|^2 . \tag{48}$$

Although it follows from Eq. (40) that the $C_{\bar{n}_r}$ coefficients depend on all quantum numbers, through their dependence on the rotation matrices, it can be shown[33] that for energy levels above $\bar{n}_c$ this dependence cancels out. We obtain the intuitively clear result that the contribution to the background flux is independent of the field direction,

$$W^{\text{background}} = \sum_{n_A \leq n \leq n_B} [1 - \exp(-W_n^c T)] \sum_{n_{2r}, m_r} |C_{\bar{n}_r}|^2 + \sum_{n > n_B} |C_n|^2 [1 - \exp(-W_n^c T)] \sum_{n_2} \exp(-W_{\bar{n}_z}^V \tau) . \tag{49}$$

The above equations enable one to calculate the ionization rates for the three relative field orientation of interest, symbolically denoted $(||)$, $(//)$, and $(|/)$. The wealth of experimental data[19] available for all these orientations,

constitutes a sensitive probe of our theory. In Sec. IV we examine the model developed here, by directly comparing it with experiments. As shown below, the observed features are, more often than not, in good quantitative
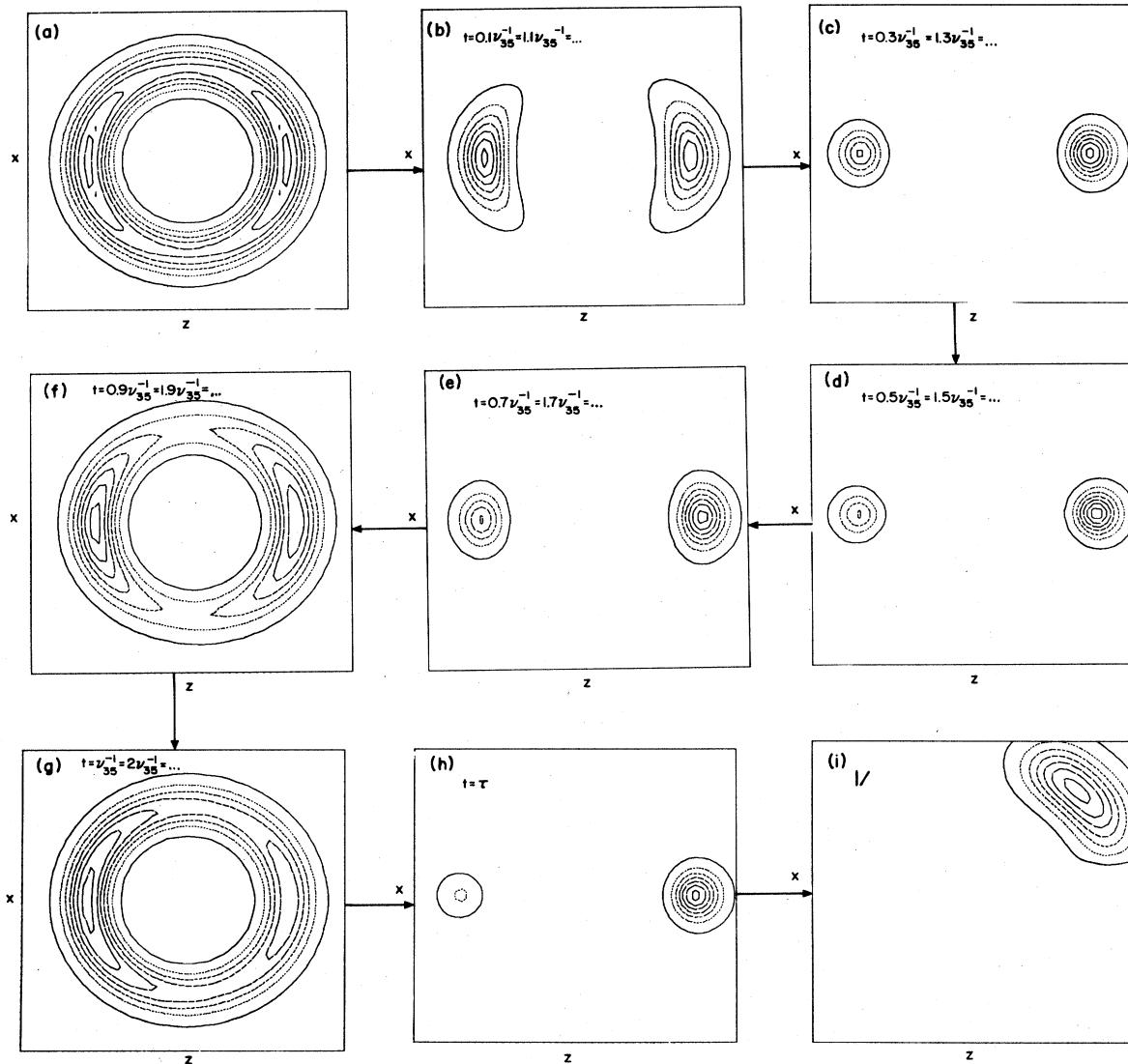
FIG. 9. Temporal evolution of the $n = 35$ wave packet ($F = 100$ V/cm) (a) as it exists from the foil ($t = 0$), (b)—(g) at subsequent times, (h) as it exits from the variable-field region ($\tau = 0.71$ nsec), (i) after ionization in a 680 V/cm, rotated spectrometer field.

agreement with our theory. This is despite the fact that some parameters associated with wavepacket preparation in the beam-foil encounter are not really known.

IV. RESULTS AND DISCUSSION

One of the puzzling experimental findings[19(b)] is the apparent symmetry [see Fig. 8(c)] of the ionization signal with respect to the variable-field sign. This finding is puzzling because, in general, the ionization curve should have no such symmetry. As shown in Fig. 7, where a

wave packet in the $n = 35$ manifold is studied, the behavior of the system in the parallel and antiparallel cases is actually quite different. Plots of the wave packet as it exits from the variable-field region [Figs. 7(a)—7(d)] and in the spectrometer region [Figs. 7(e) and 7(f)] show that the variable field always tends to deplete sublevels whose charge density is localized in the negative-field direction. This results [see Figs. 7(e) and 7(f)] in a smaller ionization signal when the fields are parallel (since the spectrometer acts on an already depleted population) as compared to the antiparallel situation (in which the easily
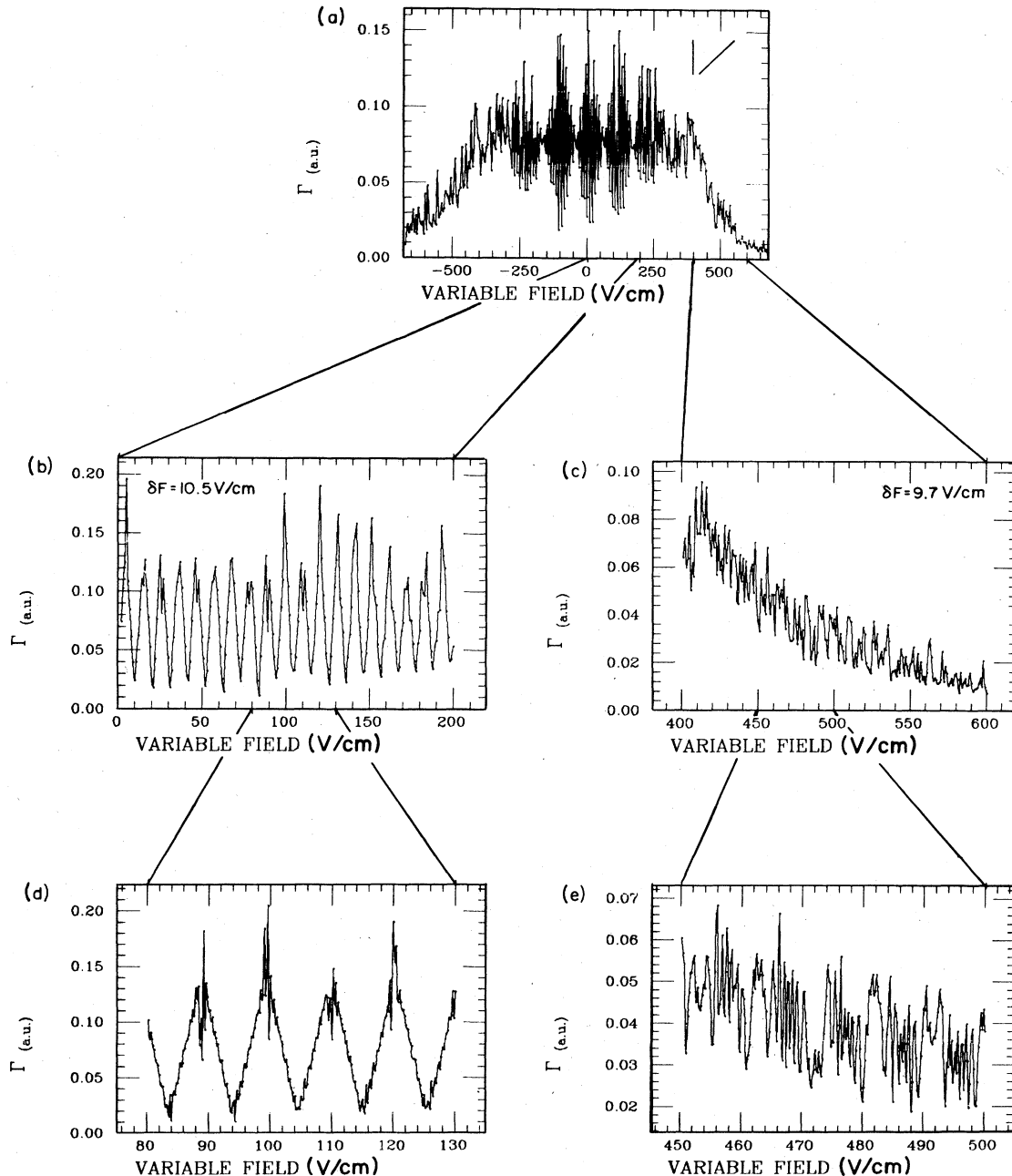
FIG. 10. Ionization yield as a function of variable-field strength. $n = 35$, with the same parameters as in Fig. 1.

ionized levels have not been depleted in the variable-field region).

What brings about the apparent symmetry is the dominant background ionization. As discussed in Sec. III, the background signal is due to levels above the (spectrometer) ionization barrier. Since all these levels get ionized in the spectrometer, the signal is merely a function of the population of levels surviving the variable field, and is independent of their identity or the charge distribution. Hence, the background signal is unaffected by a change of the variable-field sign.
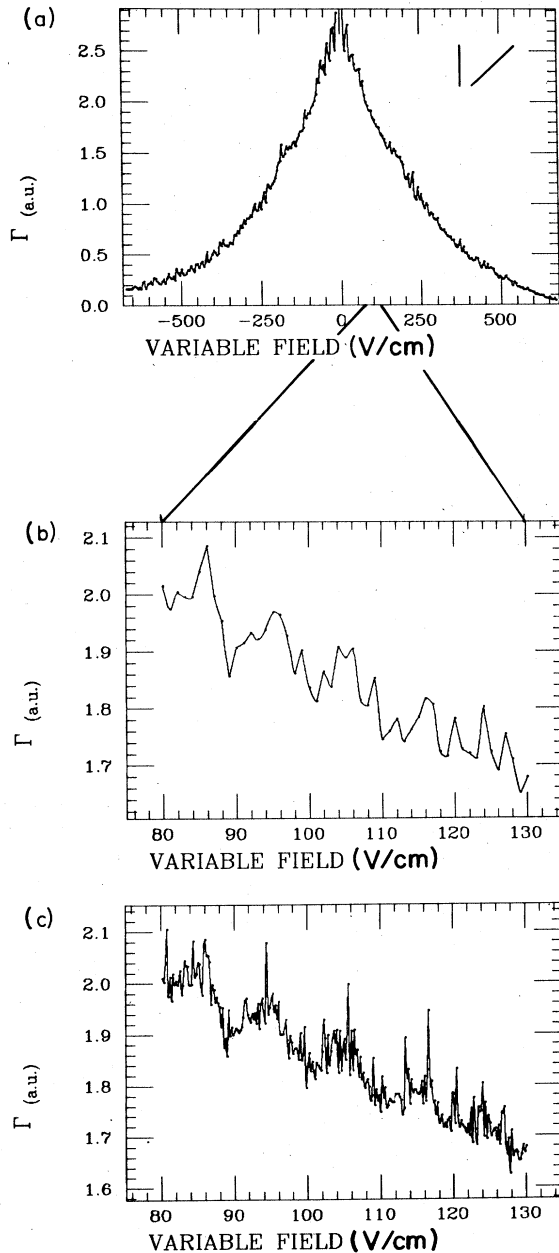
FIG. 11. Yield curve for mutually tilted fields, using the parameters given for Fig. 1.

Thus, as shown in Fig. 8, the inclusion of the background process results in excellent agreement with the tilted parallel-field experiment,[19(b)] [see Fig. 8(c)] in a seemingly symmetric ionization yield curve. An enlargement of the theoretical curve [Fig. 8(b)] reveals, however, some asymmetry at high variable fields. This effect was not discerned experimentally[19(b)] because the spectrometer fields (680 V/cm) used were not strong enough. We predict, however, that this inherent asymmetry would be observed at higher spectrometer field strengths.

The importance of the onset of the far-wings asymmetry is that it enables us to estimate the highest Rydberg level produced in the beam-foil encounter. This is so because the background signal must, as discussed above, come from the high-principal-quantum-number portion of the wave packet. The variable-field strengths at which asymmetry can be discerned is a direct function of the number of states involved. Since in the experiment of Vager et al.[19(b)] no asymmetry was detected, only a lower limit of $n \cong 90$ for the highest principal quantum number prepared can be set.

We turn our attention now to the nonparallel-fields case. As mentioned above, beat pattern which is most noticeable at high variable fields is observed in this configuration[19(b)] Figure 9 presents a series of different-times "snapshots" of the probability density $|\psi_n(t)|_F^2$ in the z-x plane. It clearly contracts and expands periodically with time. This corresponds to the rotation of a "beacon" of the three-dimensional probability density at an angular frequency $\omega = (E_{\bar{n}z}^V - E_{\bar{n}_z'}^V)$. Foregoing the accurate treatment presented below, we can estimate this frequency in the low-field region by using the first-order perturbation expression for the energy,

$$E^1 \sim 3Fn(n_1 - n_2)/2 .$$

It follows that for $n'_{2z} = n_{2z} + 1$,

$$\omega_0 \sim 3Fn . \tag{50}$$

The beat pattern can be monitored at any given time τ by varying the field strength. To a first approximation, it follows from Eq. (50) that the field periodicity is given by

$$\delta F_0 \sim 2\pi/(3\tau n) . \tag{51}$$

In Fig. 10 we present computations of the ionization signal, as a function of the variable-field strength, for the mutually tilted fields ($|/$) case. In order to identify the respective roles played by $n = n'$ versus $n \neq n'$ interferences in producing the observed beat pattern, we have confined this study to a manifold composed of a single ($n = 35$) principal quantum number. The ionization signal is now given directly by Eq. (47). Using the first-order expression for the field period, Eq. (51), with $\tau = 0.71$ nsec and $n = 35$, we obtain a field period of 10.5 V/cm, which, as shown in Fig. 10(b), coincides with the more exact treatment of Eq. (47) at relatively weak (0—200 V/cm) variable fields.

At high fields, deviations from Eq. (51), due to second- and higher-order effects, are detectable. The second-order correction to the energy levels,

$$E^{(2)} \sim -F^2 n^4 [17n^2 - 3(n_1 - n_2)^2 - 9m^2 + 19]/16 , \quad (52)$$

results in an improved expression for the field periodicity,

$$\delta F \sim 4\pi / [6n + 3n^4 F(n - 2n_2 - 2)\tau] \quad (53)$$

for $n_2' = n_2 + 1$. For small n_2 this equation predicts a *decrease* of the period with increasing field strengths. This, as shown in Fig. 10(c), is indeed the case; $\delta F = 9.7$ V/cm for $F \cong 500$ V/cm, as compared to 10.5 V/cm for $F \cong 100$ V/cm.

The decrease in δF is accompanied by a secondary structure. This is shown in Fig. 10(d), in which the oscillations at low fields are plotted on a finer field scale. The secondary structure, given to second order by Eq. (53), is due to the n_2 dependence of the field periodicity. As shown in Fig. 10(e), this structure becomes dominant at higher fields. As discussed below, this effect has been measured experimentally[19] [see Fig. 12(c)] and found to be in full agreement with present theory.
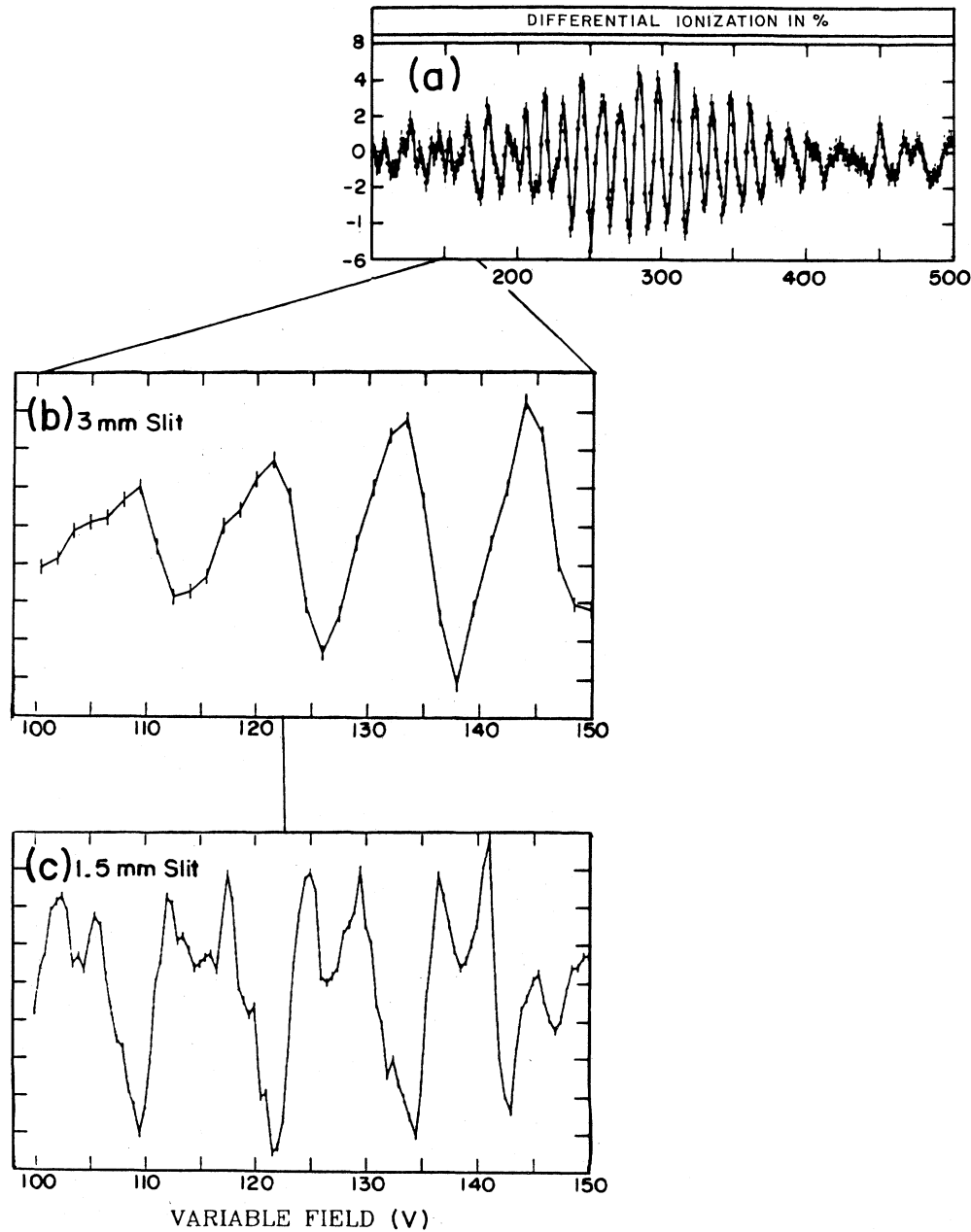
FIG. 12. Experimental differential yield curve. $F^s = 450$ V/cm, $1 = 9.9$ cm, $E_p = 2$ MeV ($\tau = 5.06$ nsec). (b) An improved resolution section. (c) A further twofold improvement in resolution.

The ionization signal due to the full (all n) wave packet, in the mutually tilted fields case, is given in Fig. 11. The most noticeable difference from the single-n case is the addition of the smooth background signal. Of greater interest is the observation that as the longitudinal field varies, different principal quantum numbers dominate the calculated beat pattern. Basically, as the field increases the range of partially depleted n levels (giving rise to the oscillatory behavior) moves to lower and lower values of n. In addition, within each such manifold, the period is dominated by no more than two or three consecutive sublevels—the ones decaying most slowly in the variable-field region. As a result, the beat pattern of Fig. 11 is dominated by the fundamental and the second harmonics.

Detailed comparisons of this theory with experiments are best done by considering the *differential* yield (dW/dF) as a function of F. The most detailed experiments[19(b)] were performed using somewhat different parameters than those of Fig. 11. The measured differential yield for an experimental arrangement for which $F^s = 450$ V/cm and $\tau = 5.06$ nsec is shown in Fig. 12. The results of the present model for the same set of parameters are presented in Fig. 13, where we again concentrate temporarily in a single principal quantum number. The
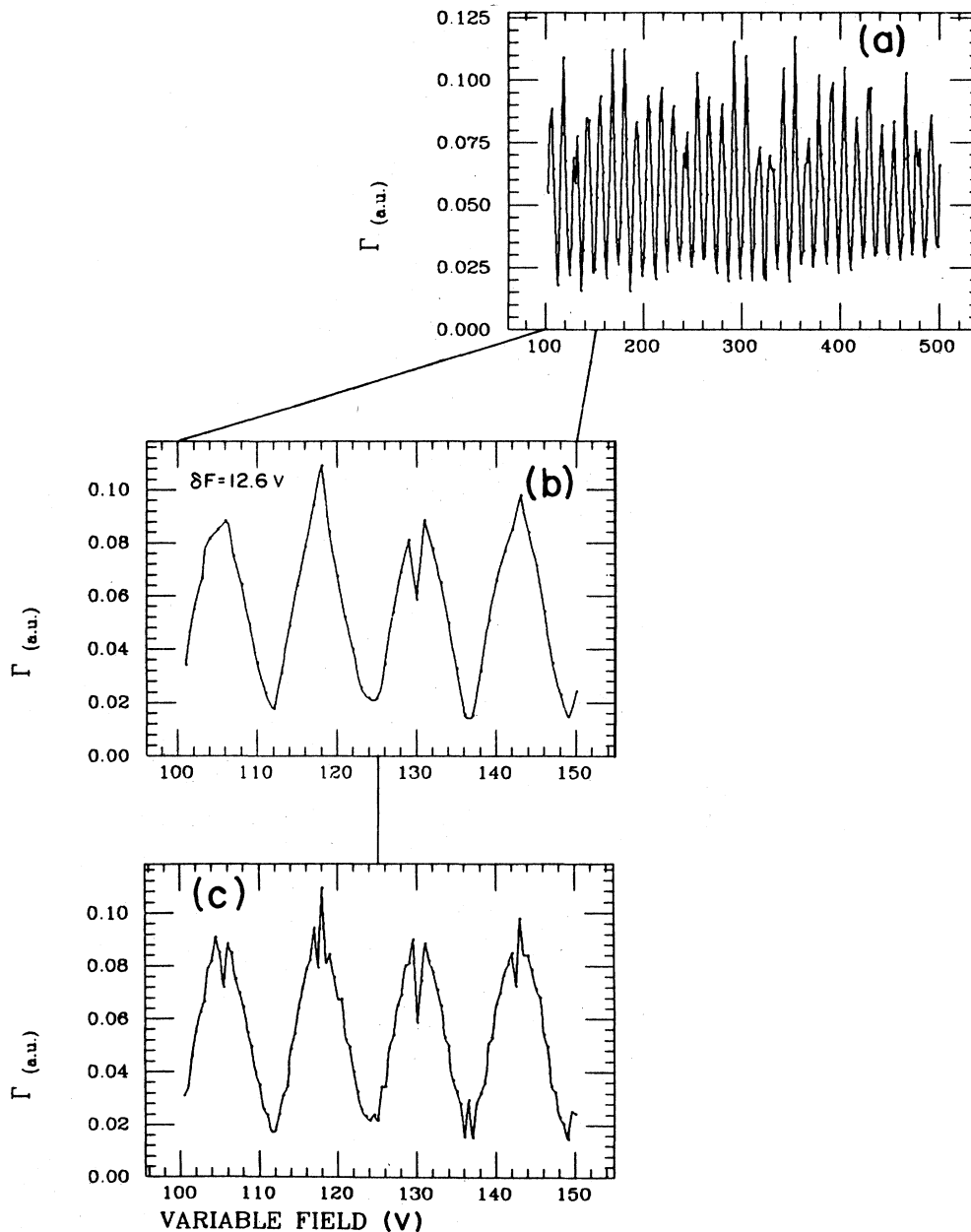
FIG. 13. Calculated curve using the parameters of Fig. 12, $n = 41$, (b) twice, (c) four times the density of data points.

choice of $n = 41$ is due to this level's lying at the center of the range of tunneling-energy levels bounded by the spectrometer field intensity. Thus for this state the largest number of sublevels contribute to the interference effect. The same is true for $n = 35$ at a spectrometer field strength of 680 V/cm. Figure 13 shows that our theory agrees with experiment with respect to the coarse [Figs. 13(a) and 12(a)], fine [Figs. 13(b) and 12(b)], and very fine [Fig. 13(c) and 12(c)] beat patterns. Most surprising is that even the absolute phases (i.e., the field values where maxima or minima occur) are well reproduced by our theoretical model. This is despite the fact that the preparation step due to the beam-foil encounter was treated in a very simplistic way.

In conclusion it seems that the success of the simple model presented above justifies the assumption of a direct "free-bound" capture mechanism in beam-foil encounters. We succeeded in explaining the beat pattern as well as the overall appearance of the ionization-yields curve, including the near symmetry, shown here to be due to the dominance of the background signal. The success of this model clearly demonstrates that the states generated in the beam-foil encounter are indeed coherent as previously stipulated.[19(a)]

[1]A. V. Vinogradov, A. M. Urnov, and V. P. Shevel'so, Zh. Eksp. Teor. Fiz. **60**, 2060 (1971) [Sov. Phys.—JETP **33**, 1110 (1971)].

[2]K. Omidvar, Phys. Rev. A **12**, 911 (1975).

[3]R. Shakeshaft and L. Spruch, Rev. Mod. Phys. **51**, 369 (1979).

[4]M. W. Lucas, W. Steekelmacher, J. Macek, and K. E. Potter, J. Phys. B **13**, 4833 (1980).

[5]J. Rothermel, H. D. Betz, F. Bell, and V. Zacek, Nucl. Instrum. Methods **194**, 341 (1982).

[6]R. L. Brooks and H. G. Berry, Phys. Rev. A **25**, 161 (1982).

[7]S. P. Alliluev and I. A. Malkin, Zh. Eksp. Teor. Fiz. **66**, 1283 (1974) [Sov. Phys.—JETP **39**, 627 (1974)]; H. J. Silverstone, Phys. Rev. A **18**, 1853 (1978); L. B. Mendelsohn, Phys. Rev. **176**, 90 (1968).

[8]R. J. Damburg and V. V. Kolosov, J. Phys. B **9**, 3149 (1976); M. Hohenberger, H. V. McIntosh, and E. Brandas, Phys. Rev. A **10**, 1494 (1974); M. H. Alexander, Phys. Rev. **178**, 34 (1969).

[9]C. Lanczos, Z. Phys. **68**, 204 (1931).

[10]J. R. Oppenheimer, Phys. Rev. **31**, 66 (1928).

[11]M. H. Rice and R. H. Good, J. Opt. Soc. Am. **52**, 239 (1962).

[12]D. S. Bailey, J. R. Hiskes, and A. C. Riviere, Nucl. Fusion **5**, 41 (1965).

[13]J. A. C. Gallas, H. Walther, and E. Werner, Phys. Rev. A **26**, 1775 (1982).

[14]D. A. Harmin, Phys. Rev. A **24**, 2491 (1981).

[15]D. Farrelly and W. P. Reinhardt, J. Phys. B **16**, 2103 (1983).

[16]H. J. Korsch and R. Mohlenkamp, Z. Phys. A **314**, 267 (1983).

[17]D. Banks and J. G. Leopold, J. Phys. B **11**, 37 (1978).

[18]E. Luc-Koenig and A. Bachelier, J. Phys. B **13**, 1743 (1980).

[19](a) Z. Vager, E. P. Kanter, D. Schneider, and D. S. Gemmell, Phys. Rev. Lett. **50**, 954 (1983). (b) Z. Vager *et al.* (unpublished).

[20]H. A. Bethe and E. E. Salpeter, *Quantum Mechanics of One- and Two-Electron Atoms* (Academic, New York, 1957).

[21]L. H. Thomas, Proc. R. Soc. (London) **114**, 561 (1927).

[22]J. R. Oppenheimer, Phys. Rev. **31**, 349 (1928).

[23]H. C. Brinkman and H. A. Kramers, Proc. Acad. Sci. Amsterdam **33**, 973 (1930).

[24]H. Tawara and A. Russek, Rev. Mod. Phys. **45**, 178 (1973).

[25]J. Palinkas, R. L. Watson, G. Pedrazzini, D. Church, and R. Kenefick, Nucl. Instrum. Methods A **240**, 498 (1985).

[26]J. E. Bayfield, Proceedings of the Fourth International Conference on Atomic Physics, Heidelberg, Germany, 1975 (unpublished).

[27](a) J. F. Reading, A. L. Ford, and R. L. Becker, J. Phys. B **14**, 1995 (1981). (b) J. F. Reading, A. L. Ford, and R. L. Becker, J. Phys. B **15**, 625 (1982).

[28]H. D. Betz and D. Roschenthaler, Phys. Rev. Lett. **50**, 34 (1983).

[29]K. O. Groeneveld, *Molecular Ions, Geometric and Electronic Structures*, Vol. 90 of NATO ASI Series, edited by J. Berkowitz and K. O. Groeneveld (Plenum, New York, 1983), p. 423; E. P. Kanter, *ibid.* p. 463; J. Remillieux, *ibid.* p. 445; B. J. Zabransky, P. J. Cooney, D. S. Gemmell, E. P. Kanter, and Z. Vager, Rev. Sci. Instrum. **54**, 531 (1983).

[30]H. G. Berry, L. Engstrom, R. Hellborg, S. Huldt, C. Jupen, A. Trigueiros, and I. Martinson, Phys. Lett. **97A**, 187 (1983); I. Martinson, Nucl. Instrum. Methods **202**, 1 (1982).

[31]C. J. Woods, N. E. B. Cowern, L. B. Bridwell, and C. J. Sofield, J. Phys. B **1**, 4113 (1985).

[32]L. D. Landau and E. M. Lifshitz, *Quantum Mechanics: Non-Relativistic Theory* (Addition-Wesley, New York, 1965).

[33]T. Seideman, M.Sc. Thesis, The Weizmann Institute, 1985.

[34]A. R. Edmonds, *Angular Momentum in Quantum Mechanics* (Princeton University Press, Princeton, 1960).

[35]D. Park, Z. Phys. **159**, 155 (1960).

[36]R. E. Langer, Phys. Rev. **51**, 669 (1937).

[37]M. Abramowitz and I. A. Stegun, *Handbook of Mathematical Functions* (Dover, New York, 1965).

[38]R. T. Pack, J. Chem. Phys. **60**, 638 (1974).

[39]R. D. Levine, *Quantum Mechanics of Molecular Rate Processes* (Clarendon, Oxford, 1969).